Optimization of Land Area Mapping and Volume Calculations using Drone Lidar Livox Mid-40 Data with the Downsampling Method

Adhitya Surya Manggala[1], *Ervina* Ahyudanari[2], *Mokhamad Nur* Cahyadi[3], *Agus Budi* Raharjo[4], *Zambri* Harun[5] and *Maria Lea Escantilla* Lebuna[6]

[1,2]Department of Civil Engineering, Institut Teknologi Sepuluh Nopember, Surabaya, Indonesia
[3]Department of Geomatics Engineering, Institut Teknologi Sepuluh Nopember, Surabaya, Indonesia
[4]Department of Informatics Engineering, Institut Teknologi Sepuluh Nopember Surabaya, Indonesia
[5]Department of Mechanical and Materials Engineering, Uniersiti Kebangsaan Malaysia, Selangor, Malaysia
[6]College of Agriculture and Forestry, West Visayas State University, Philippines

Abstract. One reason for the growing acceptance of 3D point cloud-based research and applications is the quick advancement of 3D scanning technologies. However, there are still a number of serious issues that have an impact on point cloud utilization performance. Among these difficulties are controlling the quantity of points, irregular point density, and a deficiency of location proximity data. In this study, we use Livox Mid-40 Drone Lidar Data and a downsampling technique to compute land area and volume. However, it can be highly challenging and time-consuming to extract usable information from enormous amounts of gathered data. Motivated by these results, this study recommends using downsampling approaches to minimize the size of the final data set while preserving data integrity, which will facilitate and expedite. The Livox Mid-40 Lidar Drone data was optimal at 00:00:30 with a flying height of 75,719 meters and a measurement diameter of 50.3 meters. By using downsampling techniques, the number of points can be reduced by up to 40 percent from the previous number of data points. Meanwhile, the data size can be 10 percent smaller than the original data. To calculate the area of land of the same size, there is a difference of 0.53 square meters. Meanwhile, for the calculation of cubic volume, there is a difference of 1.63 cubic meters.

Keywords: Optimization, Land Area Mapping, Volume Calculations, Drone Lidar Livox Mid-40 Data, Downsampling Method

1 Introduction

Sustainable land usage and management require optimized land area mapping [1]. It entails determining how best to manage land in order to optimize advantages and reduce

detrimental effects on the environment and society. The initialization of the optimization method is one of the issues in land area mapping [2] optimization, and it can have a big impact on the results. Furthermore, multi-objective [3] is required due to the multitude of considerations associated with land use planning in order to provide decision-makers with a range of options for additional investigation. The optimization of land area mapping yields time and cost savings [1]. Land cover mapping becomes more economical when time and resources are saved through automation and optimized processes in geospatial data services [4].

Different techniques exist for calculating land volume, such as aerial scanning grid and composite methods [5]. The composite approach re-triangulates a new surface using points from both surfaces, whereas the grid method divides the land into a grid and determines the volume of each cell. Digital terrain models [6], which are used to compute the amount of material that was mined or piled up in the area [7], can be created using aerial photography or terrestrial scanning [8]. The volume of a landfill is determined using land fill volume calculators, which is essential for effective waste management [9]. Precise computations of land area are necessary for well-informed decision-making, resource distribution, and environmental oversight[10].

With the advent of Lidar drones, Lidar (Light Detection and Ranging) technology—which has historically been utilized in portable sensors, aerial sensors aboard aircraft, and satellite-based systems—has experienced notable developments [11]. These drones are outfitted with Lidar sensors, which measure distances with astounding accuracy using laser light. This allows for the construction of intricate 3D maps of the area beneath [12]. Due to the adaptability and efficiency these drones offer across a variety of sectors, including industrial inspections, surveying, mapping, construction, forestry, agriculture, and infrastructure development, the worldwide Lidar drone market is anticipated to rise rapidly. Lidar drones are essential for producing accurate three-dimensional (3D) models of vital infrastructure, which support planning, building, and maintaining operations while guaranteeing efficiency and safety [13].

Lidar sensor integration with drone platforms[14], like the DJI M300, offers a flexible basis for peak performance. Due to these advancements, the number of businesses using drones fitted with Lidar as comprehensive, full-scale 3D mapping systems that can accurately cover enormous areas has rapidly increased [15]. Lidar drones have, in general, transformed geospatial technology by providing accurate solutions for a variety of businesses and applications [16]. With advancements in sensor capacities, data processing algorithms, and integration with other remote sensing technologies, drone LiDAR technology is still developing. By giving precise and in-depth spatial data from above, it offers insightful information for several businesses [17].

To create a point cloud, the gathered LiDAR data—which includes positional data, intensity values, and distance measurements—is processed [18]. The surveyed area is represented in three dimensions by the point cloud, where each point denotes a place on Earth's surface that was measured using a laser. In order to produce digital elevation models (DEMs), contour maps, and other geospatial outputs, point cloud data can be further examined and processed. LiDAR data is useful for precise terrain modeling and feature extraction because to its high density and accuracy.

A LiDAR sensor produced by Livox, the Mid-40 is renowned for its affordability and industrial-grade performance, which makes it appropriate for a range of uses such as security, mapping, mobile robotics, and more [19]. It provides excellent dependability and a detection range of 260 meters at 80% reflectivity [20]. At a wavelength of 905 nm, the sensor generates laser light, which is reflected off objects and picked up by the receiver. The sensor has 360° spherical scan coverage thanks to its stepper motor-driven pitching and yawing mechanisms, which enable it to revolve in 3D space [21].

In LiDAR data, downsampling is the act of deleting or aggregating points in order to reduce the density of point clouds [22]. Reducing the bulk of the data, accelerating processing, and preserving the harmony between computing efficiency and data resolution are only a few advantages of this. Downsampling makes handling big LiDAR datasets easier by enabling more effective data processing and storage [23]. In order to provide more effective processing and analysis of LiDAR data for a variety of applications, the objective is to preserve important information while minimizing the total data size. Downsampling makes handling huge datasets easier and enables more effective data processing and storage by reducing the volume of LiDAR data while maintaining important information[24].

This research will discuss the optimization of Livox Mid-40 Lidar data integrated with the DJI M300 drone in measuring land area and calculating land volume. Apart from that, this research will explore LiDAR data using the downsampling method so that smaller data sizes can be produced, while still striving for good data accuracy like the original data.

2 Methodology

2.1 Point Cloud Data

The processing and analysis of 3D point cloud data, which is a frequently used format for describing geometric information in 3D space without any discretization, is referred to as 3D point cloud-based research. A point cloud is a collection of unordered points in three dimensions that can be used to create a specific three-dimensional shape. These points are represented by coordinates on the x, y, and z axes. With a 3D scanner, such the previously described RGB-D cameras or LiDAR, the coordinates of these points can be acquired from one or more perspectives [25].

Deep learning techniques can be applied to a variety of point cloud processing tasks by using 3D point voxels, which offer a straightforward and efficient means of representing and processing 3D point cloud data [26]. This representation has ramifications for a wide range of applications, including those in infrastructure and construction, and has demonstrated promise in overcoming difficulties in scene understanding.

When downsampling LiDAR data using a voxel grid approach, the equation to calculate the centroid of points within each voxel involves determining the average position in three-dimensional space [27]. Let's denote a voxel as Vi and its centroid as Ci(x,y,z), where x, y, and z are the coordinates of the centroid. The centroid coordinates can be calculated using the following equations:

$$C_{\bar{l}_x} = \frac{\sum_{j=1}^{N_i} x_j}{N_i} \text{; X – coordinate of Centeroid } (C_{\bar{l}_x}) \quad (1)$$

$$C_{\bar{l}_y} = \frac{\sum_{j=1}^{N_i} y_j}{N_i} \text{; Y – coordinate of Centeroid } (C_{\bar{l}_y}) \quad (2)$$

$$C_{\bar{l}_z} = \frac{\sum_{j=1}^{N_i} z_j}{N_i} \text{; Z – coordinate of Centeroid } (C_{\bar{l}_z}) \quad (3)$$

Equation (1) where N_i is the number of points within voxel V_i and x_j is the X-coordinate of the *j*-th point within the voxel. Equation (2) where y_j is the Y-coordinate of the *j*-th point within the voxel. Equation (3) where z_j is the Z-coordinate of the *j*-th point within the voxel. All of the equations represent the average position of the points within the voxel along each coordinate axis. The centroid coordinates Ci(x,y,z) provide a representative position for the voxel, and this downsampling method is commonly used in LiDAR data processing.

2.2 LIDAR-Based Point Cloud Data

A LiDAR device is a device that allows image scanning. Image scanning is a process that involves optically reading images and transforming them into data, information, and objects. When an object is exposed to a laser beam at predetermined intervals, LiDAR uses the distance measured and the direction of the reflected laser to represent the object's shape in a set of three-dimensional coordinates. This method yields points with 3D X, Y, and Z coordinates along with geospatial data. Each component point is created at the location where the object's reflection of the LiDAR's laser is detected [12].

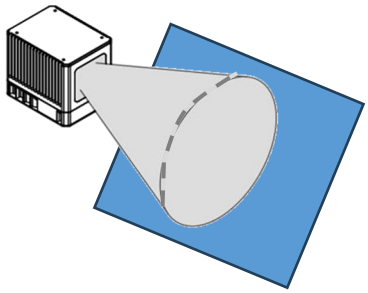

Fig. 1. The radar longitudinal section schematic diagram.

Target items may be detected inside the field of view (FOV) of LiDAR sensors . Not every target object in the field of view can be identified, though. For instance: If the reflected light is too weak to be detected, which is frequently the result of the target being too far away from the sensor or having a low reflectivity [28]. Only a portion of FOV can be illuminated by laser beams in a finite amount of time, which is related to the distribution of the scanning pattern. The target object won't be detected if the laser doesn't illuminate it. Through careful planning of the Livox LiDAR sensors' scanning technique, the percentage of FOV that is illuminated by laser beams:

$$C = \frac{Total\ area\ illuminated\ by\ laser\ beams}{Total\ area\ in\ FOV} x\ 100\% \qquad (4)$$

Point cloud data must be translated from a rectangular coordinate system to a polar coordinate system in order to process laser beams at the same angle. where q is the included angle between the point and the front of the vehicle and r is the horizontal distance between the point and the radar centre.

$$r = \sqrt{x^2 + y^2} \qquad (5)$$

$$\theta = arctan\frac{y}{x} \mathrm{x} \frac{180}{\pi} \qquad (6)$$

Laser pulses are directed toward the earth by the LiDAR sensor [29]. These laser pulses are released quickly one after the other, frequently thousands of pulses per second. A portion of the energy released by the laser pulses is reflected back to the LiDAR sensor when they strike the Earth's surface[30]. It is measured how long it takes for the laser pulses to reach the earth and back. The LiDAR sensor determines the distance between itself and the ground surface by timing the return of the laser pulses. We call this procedure Time-of-Flight. A single laser pulse can yield several returns when used by aerial LiDAR devices. This function enables the sensor to capture data about various characteristics or objects within the laser beam at various heights. Furthermore, certain LiDAR sensors record intensity data, which might reveal details about the surfaces' properties or reflectance. Usually, an Inertial Measurement Unit (IMU) and a GPS receiver are incorporated with the LiDAR system[31].

Accurate positioning data is provided by the GPS, and during data acquisition the aircraft's attitude and orientation are recorded by the IMU.[32]

2.3 The Livox Mid-40 LiDAR sensor

This sensor delivers extremely exact information in the field of view (FOV) by using an innovative non-repetitive scanning pattern to detect objects up to 260 metres away. For increased performance and flexibility, customers can include units into pre-existing designs with ease because to their compact bodies. In order to enable applications in autonomous driving, robotics, mapping, security, and other fields ranging from small batch testing to large-scale implementations, the Mid-40 has been mass-produced and is prepared for shipping right now [33].

$$x = \mathrm{r} \times \sin(\theta) \times \cos(\theta) \quad (7)$$
$$y = \mathrm{r} \times \sin(\theta) \times \sin(\theta) \quad (8)$$
$$z = \mathrm{r} \times \cos(\theta) \quad (9)$$

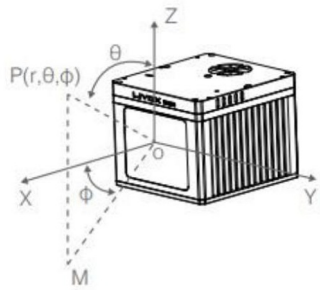

Fig. 2. Define the Livox Mid-40 lidar sensor's azimuth (ϕ) and zenith (θ) angular measurements to point P in relation to its Cartesian reference coordinate system.

Figure 2 below displays a portion of a screenshot of the point cloud sequences. The azimuth coordinate parameters provided by Livox are represented in the range of -180°~180°, where -180°~0° is equivalent to 180°~360° in the standard coordinate system. The azimuth range based on the standard coordinate system is 0~360° [34].

The Livox® Mid-40 operates in a rosette-style scan pattern for three seconds. Each circle shows the accumulation of one second's worth of data from a stationary scanner observing a stationary target surface, going from left to right. Ten thousand points are generated every second at this point [35].

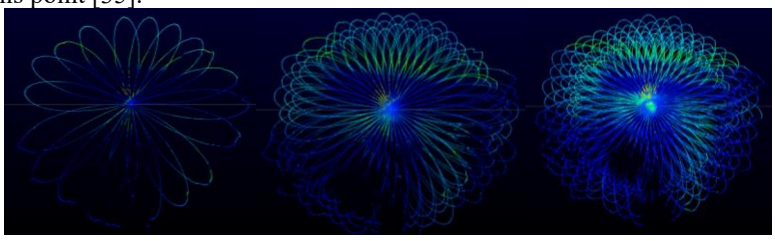

Fig. 3. Rosette Scan Pattern Non-Repeating for Livox MID-40 Sensor

2.4 Drone Integration The Livox Mid-40

LiDAR Livox MiD 40 and a camera are coupled with the DJI M300 drone sensors through payload. System the payload is capable of carrying a Livox MID 40 lidar sensor. The DJI

M300 drone can carry up to 2.7 kg (6 pounds) of cargo, but the Livox MiD 40 LiDAR weighs 0.75 kg (less than 2 pounds).

Fig. 4. Livox MID-40 Sensor integration with DJI M300 drone

The radar detector is typically installed on the vehicle's roof using a bracket to provide a wider detection range. The vehicle body points need to be removed because, depending on the vertical angle range of the laser beam emission, some laser points will fall on it that are unable to convey the features of the surrounding environment and could be misinterpreted as obstacle point clouds, which would interfere with the vehicle's ability to drive normally. According to the vehicle's length, width, and radar installation location, only the measurement points falling inside the vehicle body range that is, all the measurement points meeting the requirements of the following equation need to be filtered out [36].

$$-\frac{L}{2} - d \leq x \leq \frac{L}{2} + d \quad (10)$$

$$-\frac{W}{2} \leq y \leq \frac{W}{2} + d \quad (11)$$

$$-H \leq z \leq 0 \quad (12)$$

where L and W are, respectively, the length and width of the vehicle; H is the radar mounting height; d is the difference distance from the radar center to the center of the vehicle length; x denotes the x-axis coordinate value; and y denotes the y-axis coordinate value.

2.5 Point Cloud Downsampling

Large point clouds produced by LiDAR make it challenging and time-consuming to perform operations like segmentation, registration, and three-dimensional reconstruction. It takes sampling to reduce the load. Sampling is typically the first stage in 3D point cloud pre-processing. The pre-processing stages additionally take into account other procedures like filters and outlier removal. procedure point clouds by starting with a quick and effective downsampling procedure [37].

By clustering points within voxel volumes, a technique known as voxel grid downsampling is utilised to lower the density of point clouds. When downsampling a voxel grid, the computational time is usually (N), where N is the number of points. Because it requires spatial segmentation, voxel grid downsampling is effective at processing big point clouds more quickly. The size of the voxel grid that is employed affects processing time.

To filter point clouds using hierarchical representations, it suggest utilising a standard 3D voxel grid (rather than a 2D raster) that has previously been discretized of the continuous domain. The application of mathematical morphology with the 3D data is made possible by this intermediary representation. After morphological filtration, it reproject the outcomes into the continuous domain [27].

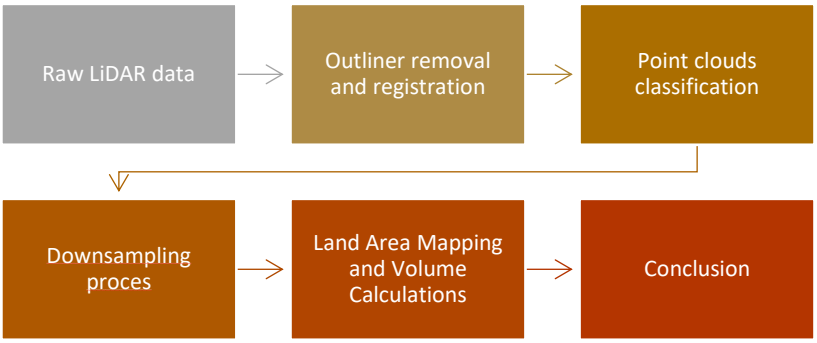

Fig.5. Research Flow for Data Collection and Processing

In order to carry out further processes like segmentation, object detection, and classification, processing a 3D point cloud requires the use of algorithms for registration, sampling, and outlier removal, as well as compression methods. The raw point clouds are the data that are obtained via LiDAR or photogrammetry.

3 Result and analysis

The data used in this research was obtained from data collection using a DJI M300 drone and a Livox Mid-40 LiDAR sensor, which was carried out during the drone's initial launch event in Tambak Area, Pandan, District. Galis, Pamekasan Regency, East Java, is geographically located at 7°12'02.0"S and 113°32'56.6"E. In collecting this data, data was collected by flying the drone at a height of 75 meters and a measurement diameter of 50 meters. Data is recorded by the Livox Mid-40 LiDAR sensor vertically from the ground to the target height.

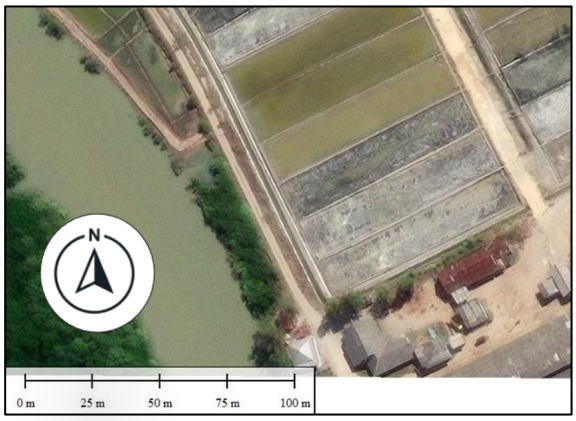

Fig. 6. Research Sites

3.1 Point Cloud Processing

Based on this research, raw data was obtained in the form of RAW LiDAR Data with recording for several minutes. From this raw data, there is the most optimal data, namely data recording, diameter coverage area, an altitude, account of points, frame time and size of the LiDAR data measurement memory.

Table 1. RAW LiDAR Data Parameters

Parameter	Value	Units
Time recording	00:00:30	Seconds
diameter coverage	50.3	meters
altitude	75,719	meters
data	300,301	points
frame time	3,000	milliseconds

For data processing and analysis, the raw data from the Livox Mid-40 LiDAR sensor includes particular parameters. These settings include the angle between parallel planes, minimum roof plane area, shared points for coincident planes, height threshold, mask resolution, flat height threshold, normal distance threshold, and ground height from a Digital Elevation Model (DEM) [38]. The Livox Mid-40's raw LiDAR data set is a three-dimensional array with measurement time, channel, and range bin dimensions. It contains the raw LiDAR data as measured, together with analogue and photon-counting signals [39].

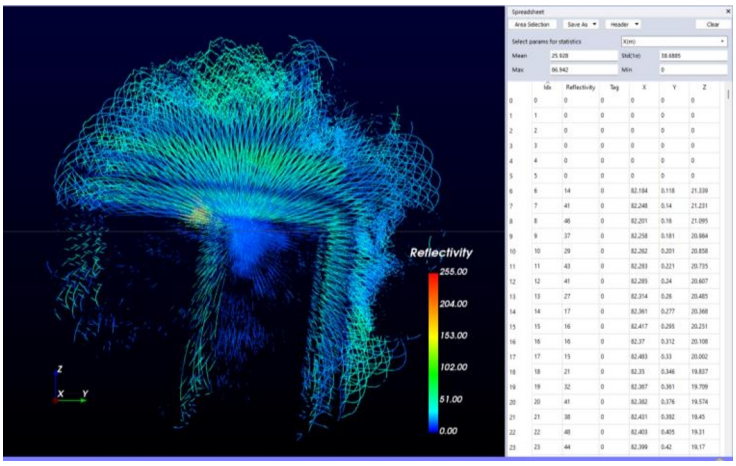

Fig. 7. RAW LiDAR Data from the Livox Mid-40 sensor

3.2 Outliner removal and Registration

These point clouds must first be aligned and combined in a common coordinate frame, which is called registration. Outlier-removal techniques are used to remove the noise and outliers present in the point clouds, while sampling or compression methods are applied to reduce the size of the point clouds.

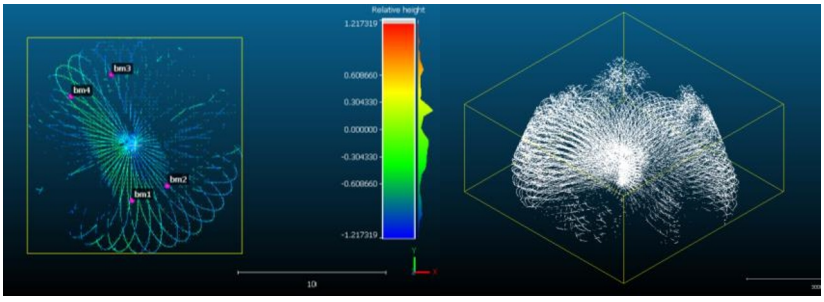

Fig. 8. LiDAR Data Georeferencing Process

At this stage georeferencing is also carried out, namely the process of labeling coordinates in the form of calibrating the position of raster data in the form of images. As reference data, these coordinates are derived from land measurements. Livox MID 40 data becomes a global coordination system even though it still contains local coordinate data from a measurement [28]. By using this technique, all local observation data is combined into a single coordinate system. Low Cost GNSS measurements are used as reference points for georeferencing [40]. To correctly match geographic data with satellite image data, it is necessary to align it with the coordinates of the measurements that have been made.

4 Discussion

Variables in the context of LiDAR data are characteristics or traits that are taken out of the point cloud data. Applications such as fuel models, forest inventory, and urban scene classification can all make use of these variables. Regression analysis, support vector machines, random forests, and other machine learning approaches can be used to assess the significance of these variables.

Table 2. Input data format of LiDAR data

Variables	**Units**
Coordinates (X, Y, Z)	Meters (m)
Intensity	Arbitrary Units (AU)
Return Number	Dimensionless
Number of Returns	Dimensionless
Scan Angle	Degrees (°)
Time Stamp	Seconds (s) or milliseconds (ms)
Classification	Dimensionless
Voxel Grid Parameters	Meters (m)
Spatial Resolution	Points per unit area (points/m²)
Temporal Resolution	Seconds (s) or milliseconds (ms)

Calculating the area of 15 x 80 metres of land for a single salt field served as measurement validation. Manual computations yield Low Cost GNSS data with a 150 square metre discrepancy from field observations. This is due to the fact that the fields are highly impacted by the weather since they lack a set land area due to their semi-permanent construction. Because of the different points of reference between the two, there is a noticeable difference in the Low-Cost GNSS form factor when compared to the LiDAR Livox MID 40. There is a local reference for LiDAR Livox Mid-40 data, and a WGS 84 reference that has been translated to UTM 49 S coordinates for Low-Cost GNSS data.

Table 3. Land Area Measurement GNSS and LiDAR Livox Mid-40

Measurement	**Low Cost GNSS**	**LiDAR Livod Mid-40**
Area	2,550 m^2	2,542 m^2
Volume	2.8049 m^3	93.3431 m^3

Furthermore, fields are among the data objects that the LiDAR Livox Mid-40 has identified. At 5.91%, the measurement error data for land is better corrected. Because LiDAR data can map the topography in more detail, measurements made with the LiDAR Livox Mid-40 have a higher degree of precision [41]. LiDAR offers both absolute and relative accuracy, enabling more realistic interpretation and improved modelling. This is employed in

acquisition processes, like figuring out item heights and identifying land borders and surrounding bodies of water.

Table 4. Normalised Measurement Level according to Land Area

Low Cost GNSS	LiDAR Livod Mid-40
6.25 %	5.91 %

The results of LiDAR data processing using downsampling methods depend on the specific downsampling technique applied and the parameters chosen. Downsampling is typically used to reduce the density of point clouds, making them more manageable while retaining key features for certain applications.

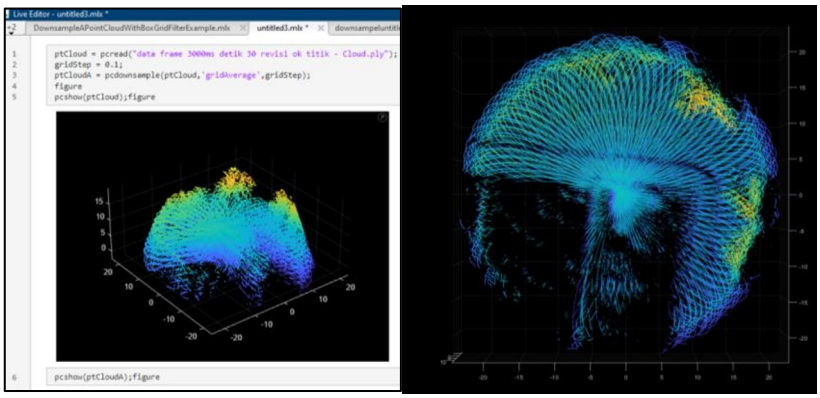

Fig. 9. Results of Data Processing using the Downsampling Method

In voxel-based downsampling, the terrain features may be smoothed as only the centroids of voxels are retained [42]. This could result in a loss of fine-scale details in the terrain. Like uniform grid downsampling, aim to create a more uniform distribution of points across the area, which can be beneficial for certain applications.

Table 5. Downsampling Analysis

Analysis	before downsampling	after downsampling
Point Cloud	300,301 points	181,787 points
Data size	2.08 Megabytes	1.84 Megabytes
Land area	1,029.00 m^2	1,028.47 m^2
Cubic volume	1,923.36 m^3	1,924.99 m^3

The primary result of downsampling is a reduction in the number of LiDAR points. This reduction can significantly decrease the overall size of the data [37], making it more computationally efficient for subsequent analysis. Downsampling involves a trade-off between maintaining detail and increasing computational efficiency [43]. The choice of downsampling method and parameters influences the level of detail retained in the processed data. Depending on the downsampling method used (e.g., voxel grid downsampling) [42], fine-scale terrain details may be smoothed, and the dataset may represent a more generalized version of the terrain.

5 Conclusion

The Livox Mid-40 Lidar Drone data was optimal at 00:00:30 with a flying height of 75,719 meters and a measurement diameter of 50.3 meters. By using downsampling techniques, the number of points can be reduced by up to 40 percent from the previous number of data points. Meanwhile, the data size can be 10 percent smaller than the original data. To calculate the area of land of the same size, there is a difference of 0.53 square meters. Meanwhile, for the calculation of cubic volume, there is a difference of 1.63 cubic meters.

The reduced data size resulting from downsampling accelerates the speed of subsequent processing and analysis tasks. This is advantageous for applications such as feature extraction, modeling, or classification. It is essential to perform validation and quality assessment after downsampling to ensure that critical features are retained and that the processed data meets the accuracy requirements for the intended application. Downsampling can lead to improved visualization of LiDAR data, especially when dealing with large datasets. Visualization tools can handle downsampled data more efficiently.

References

[1] P. Griffiths, S. Van Der Linden, T. Kuemmerle, and P. Hostert, "Erratum: A pixel-based landsat compositing algorithm for large area land cover mapping (IEEE Journal of Selected Topics in Applied Earth Observations and Remote Sensing)," *IEEE J. Sel. Top. Appl. Earth Obs. Remote Sens.*, vol. 6, no. 5, pp. 2088–2101, 2013, doi: 10.1109/JSTARS.2012.2228167.

[2] V. Eisavi, S. Homayouni, A. M. Yazdi, and A. Alimohammadi, "Land cover mapping based on random forest classification of multitemporal spectral and thermal images," *Environ. Monit. Assess.*, vol. 187, no. 5, pp. 1–14, 2015, doi: 10.1007/s10661-015-4489-3.

[3] R. Rashdi, J. Martínez-Sánchez, P. Arias, and Z. Qiu, "Scanning Technologies to Building Information Modelling: A Review," *Infrastructures*, vol. 7, no. 4, 2022, doi: 10.3390/infrastructures7040049.

[4] M. A. Wulder *et al.*, "Operational mapping of the land cover of the forested area of Canada with Landsat data: EOSD land cover program," *For. Chron.*, vol. 79, no. 6, pp. 1075–1083, 2003, doi: 10.5558/tfc791075-6.

[5] B. Pradhan, M. N. Jebur, H. Z. M. Shafri, and M. S. Tehrany, "Data fusion technique using wavelet transform and taguchi methods for automatic landslide detection from airborne laser scanning data and quickbird satellite imagery," *IEEE Trans. Geosci. Remote Sens.*, vol. 54, no. 3, pp. 1610–1622, 2016, doi: 10.1109/TGRS.2015.2484325.

[6] C. Ginzler and M. L. Hobi, "Countrywide stereo-image matching for updating digital surface models in the framework of the swiss national forest inventory," *Remote Sens.*, vol. 7, no. 4, pp. 4343–4370, 2015, doi: 10.3390/rs70404343.

[7] A. Hamedianfar and M. Barakat A. Gibril, "Large-scale urban mapping using integrated geographic object-based image analysis and artificial bee colony optimization from worldview-3 data," *Int. J. Remote Sens.*, vol. 40, no. 17, pp. 6796–6821, 2019, doi: 10.1080/01431161.2019.1594435.

[8] K. B. Pierce, "Accuracy optimization for high resolution object-based change detection: An example mapping regional urbanization with 1-m aerial imagery," *Remote Sens.*, vol. 7, no. 10, pp. 12654–12679, 2015, doi: 10.3390/rs71012654.

[9] E. Russell, J. C. Padró, P. Montero, C. Domingo-Marimon, and V. Carabassa, "Relief Modeling in the Restoration of Extractive Activities Using Drone Imagery," *Sensors*, vol. 23, no. 4, pp. 1–15, 2023, doi: 10.3390/s23042097.

[10] L. F. F. G. Assis *et al.*, "TerraBrasilis: A Spatial Data Analytics Infrastructure for Large-Scale Thematic Mapping," *ISPRS Int. J. Geo-Information*, vol. 8, no. 11, p. 513, 2019, doi: 10.3390/ijgi8110513.

[11] M. Pełka and J. Będkowski, "Calibration of planar reflectors reshaping LiDAR's field of view," *Sensors*, vol. 21, no. 19, pp. 1–16, 2021, doi: 10.3390/s21196501.

[12] J. Będkowski and M. Pełka, "Affordable Robotic Mobile Mapping System Based on Lidar with Additional Rotating Planar Reflector," *Sensors*, vol. 23, no. 3, 2023, doi: 10.3390/s23031551.

[13] H. Wang, Y. Peng, L. Liu, and J. Liang, "Study on Target Detection and Tracking Method of UAV Based on LiDAR," *2021 Glob. Reliab. Progn. Heal. Manag. PHM-Nanjing 2021*, pp. 5–10, 2021, doi: 10.1109/PHM-Nanjing52125.2021.9612936.

[14] G. Mahajan, "Applications of Drone Technology in Construction Industry: A Study 2012-2021," *Int. J. Eng. Adv. Technol.*, vol. 11, no. 1, pp. 224–239, 2021, doi: 10.35940/ijeat.a3165.1011121.

[15] W. Tan *et al.*, "Semantic Segmentation of Uav Lidar Point Clouds of a Stack Interchange With Deep Neural Networks," *Int. Geosci. Remote Sens. Symp.*, pp. 582–585, 2021, doi: 10.1109/IGARSS47720.2021.9554610.

[16] X. Wang, "Drone-based area scanning of vegetation fluorescence height profiles using a miniaturized hyperspectral lidar system," *Appl. Phys. B*, vol. 124, no. 11, pp. 1–5, 2018, doi: 10.1007/s00340-018-7078-7.

[17] W. Wei, B. Shirinzadeh, R. Nowell, and M. Ghafarian, "Enhancing Solid State LiDAR Mapping with a 2D Spinning LiDAR in Urban Scenario SLAM on Ground Vehicles," 2021.

[18] Z. Wang, X. Wang, B. Fang, K. Yu, and J. Ma, "Vehicle detection based on point cloud intensity and distance clustering," *J. Phys. Conf. Ser.*, vol. 1748, no. 4, pp. 0–6, 2021, doi: 10.1088/1742-6596/1748/4/042053.

[19] LIVOX, "Livox Mid-40 Quick Start Guide," 2019, [Online]. Available: https://www.livoxtech.com/3296f540ecf5458a8829e01cf429798e/downloads/20190530/Livox Mid-40 Quick Start Guide multi v1.4.pdf.

[20] A. Ortiz Arteaga, D. Scott, and J. Boehm, "Initial investigation of a low-cost automotive LiDar system," *Int. Arch. Photogramm. Remote Sens. Spat. Inf. Sci. - ISPRS Arch.*, vol. 42, no. 2/W17, pp. 233–240, 2019, doi: 10.5194/isprs-archives-XLII-2-W17-233-2019.

[21] C. L. Glennie and P. J. Hartzell, "Accuracy assessment and calibration of low-cost autonomous LiDAR sensors," *Int. Arch. Photogramm. Remote Sens. Spat. Inf. Sci. - ISPRS Arch.*, vol. 43, no. B1, pp. 371–376, 2020, doi: 10.5194/isprs-archives-XLIII-B1-2020-371-2020.

[22] D. Zhang, X. Wang, Z. Zheng, and X. Liu, "Unsupervised Domain Adaptive 3-D Detection With Data Adaption From LiDAR Point Cloud," *IEEE Trans. Geosci. Remote Sens.*, vol. 60, pp. 1–14, 2022, doi: 10.1109/TGRS.2022.3226570.

[23] A. Al-Rawabdeh, F. He, and A. Habib, "Automated feature-based down-sampling approaches for fine registration of irregular point clouds," *Remote Sens.*, vol. 12, no. 7, pp. 1–25, 2020, doi: 10.3390/rs12071224.

[24] M. Amado, F. Lopes, A. Dias, and A. Martins, "LiDAR-based Power Assets Extraction based on Point Cloud Data," *2021 IEEE Int. Conf. Auton. Robot Syst. Compet. ICARSC 2021*, pp. 221–227, 2021, doi: 10.1109/ICARSC52212.2021.9429772.

[25] Z. Ding, Y. Sun, S. Xu, Y. Pan, Y. Peng, and Z. Mao, "Recent Advances and Perspectives in Deep Learning Techniques for 3D Point Cloud Data Processing," *Robotics*, vol. 12, no. 4, pp. 1–23, 2023, doi: 10.3390/robotics12040100.

[26] Y. Guo, H. Wang, Q. Hu, H. Liu, L. Liu, and M. Bennamoun, "Deep Learning for 3D Point Clouds: A Survey," *IEEE Trans. Pattern Anal. Mach. Intell.*, vol. 43, no. 12, pp. 4338–4364, 2021, doi: 10.1109/TPAMI.2020.3005434.

[27] F. Guiotte, S. Lefèvre, and T. Corpetti, "Attribute filtering of urban point clouds using max-tree on voxel data," *Lect. Notes Comput. Sci. (including Subser. Lect. Notes Artif. Intell. Lect. Notes Bioinformatics)*, vol. 11564 LNCS, no. January, pp. 391–402, 2019, doi: 10.1007/978-3-030-20867-7_30.

[28] R. G. Brazeal, B. E. Wilkinson, and H. H. Hochmair, "A rigorous observation model for the risley prism-based livox mid-40 lidar sensor," *Sensors*, vol. 21, no. 14, 2021, doi: 10.3390/s21144722.

[29] B. Liu, S. Chen, H. Huang, and X. Tian, "Tree Species Classification of Backpack Laser Scanning Data Using the PointNet++ Point Cloud Deep Learning Method," *Remote Sens.*, vol. 14, no. 15, 2022, doi: 10.3390/rs14153809.

[30] G. A. J. Kartini and I. Gumilar, "Utilization of iPad Pro LiDAR and Low-Cost GNSS Ublox F9R for Data Collection of Road Assets in the Form of 3D Models Utilization of iPad Pro LiDAR and Low-Cost GNSS Ublox F9R for Data Collection of Road Assets in the Form of 3D Models," 2021, doi: 10.1088/1755-1315/1127/1/012013.

[31] M. Nur, T. As, R. Mardiyanto, and R. Er, "Geodesy and Geodynamics Performance of GPS and IMU sensor fusion using unscented Kalman fi lter for precise i-Boat navigation in in fi nite wide waters," vol. 14, pp. 265–274, 2023, doi: 10.1016/j.geog.2022.11.005.

[32] E. S. Technology, C. Service, and C. Author, "Loosely Coupled GNSS and IMU Integration for Accurate i-Boat Horizontal Navigation," vol. 18, no. 3, pp. 111–122, 2022.

[33] C. Kelly, B. Wilkinson, A. Abd-Elrahman, O. Cordero, and H. A. Lassiter, "Accuracy Assessment of Low-Cost Lidar Scanners: An Analysis of the Velodyne HDL–32E and Livox Mid–40's Temporal Stability," *Remote Sens.*, vol. 14, no. 17, 2022, doi: 10.3390/rs14174220.

[34] D. March, A. Livox, L. Livox, R. Revised, and L. L. Livox, "Explanatory Notes on Livox Point Cloud Sequences Livox 点云序列说明," pp. 1–2, 2020.

[35] I. Elkhrachy, "Accuracy Assessment of Low-Cost Unmanned Aerial Vehicle (UAV) Photogrammetry," *Alexandria Eng. J.*, vol. 60, no. 6, pp. 5579–5590, 2021, doi: 10.1016/j.aej.2021.04.011.

[36] P. Wang, T. Gu, B. Sun, D. Huang, and K. Sun, "Research on 3D Point Cloud Data Preprocessing and Clustering Algorithm of Obstacles for Intelligent Vehicle," *World Electr. Veh. J.*, vol. 13, no. 7, 2022, doi: 10.3390/wevj13070130.

[37] W. Błaszczak-Bąk, J. Janicka, C. Suchocki, A. Masiero, and A. Sobieraj-żłobińska, "Down-sampling of large lidar dataset in the context of off-road objects extraction," *Geosci.*, vol. 10, no. 6, 2020, doi: 10.3390/geosciences10060219.

[38] M. Awrangjeb and C. S. Fraser, "Automatic segmentation of raw LIDAR data for extraction of building roofs," *Remote Sens.*, vol. 6, no. 5, pp. 3716–3751, 2014, doi: 10.3390/rs6053716.

[39] G. D'Amico, A. Amodeo, I. Mattis, V. Freudenthaler, and G. Pappalardo, "EARLINET Single Calculus Chain-technical andndash; Part 1: Pre-processing of raw lidar data," *Atmos. Meas. Tech.*, vol. 9, no. 2, pp. 491–507, 2016, doi: 10.5194/amt-9-491-2016.

[40] N. A. Correa-Muños and L. A. Cerón-Calderón, "Precision and accuracy of the static gnss method for surveying networks used in civil engineering," *Ing. e Investig.*, vol. 38, no. 1, pp. 52–59, 2018, doi: 10.15446/ing.investig.v38n1.64543.

[41] H. C. Ren *et al.*, "Study on analysis from sources of error for Airborne LIDAR,"

IOP Conf. Ser. Earth Environ. Sci., vol. 46, no. 1, 2016, doi: 10.1088/1755-1315/46/1/012030.

[42] H. Qin, H. Guan, Y. Yu, and L. Zhong, "A voxel-based filtering algorithm for mobile LiDAR data," *Int. Arch. Photogramm. Remote Sens. Spat. Inf. Sci. - ISPRS Arch.*, vol. 42, no. 3, pp. 1433–1438, 2018, doi: 10.5194/isprs-archives-XLII-3-1433-2018.

[43] S. Morsy and A. Shaker, "Evaluation of LiDAR-Derived Features Relevance and Training Data Minimization for 3D Point Cloud Classification," *Remote Sens.*, vol. 14, no. 23, pp. 1–15, 2022, doi: 10.3390/rs14235934.